nature
structural biology

may 1997
volume 4 no. 5

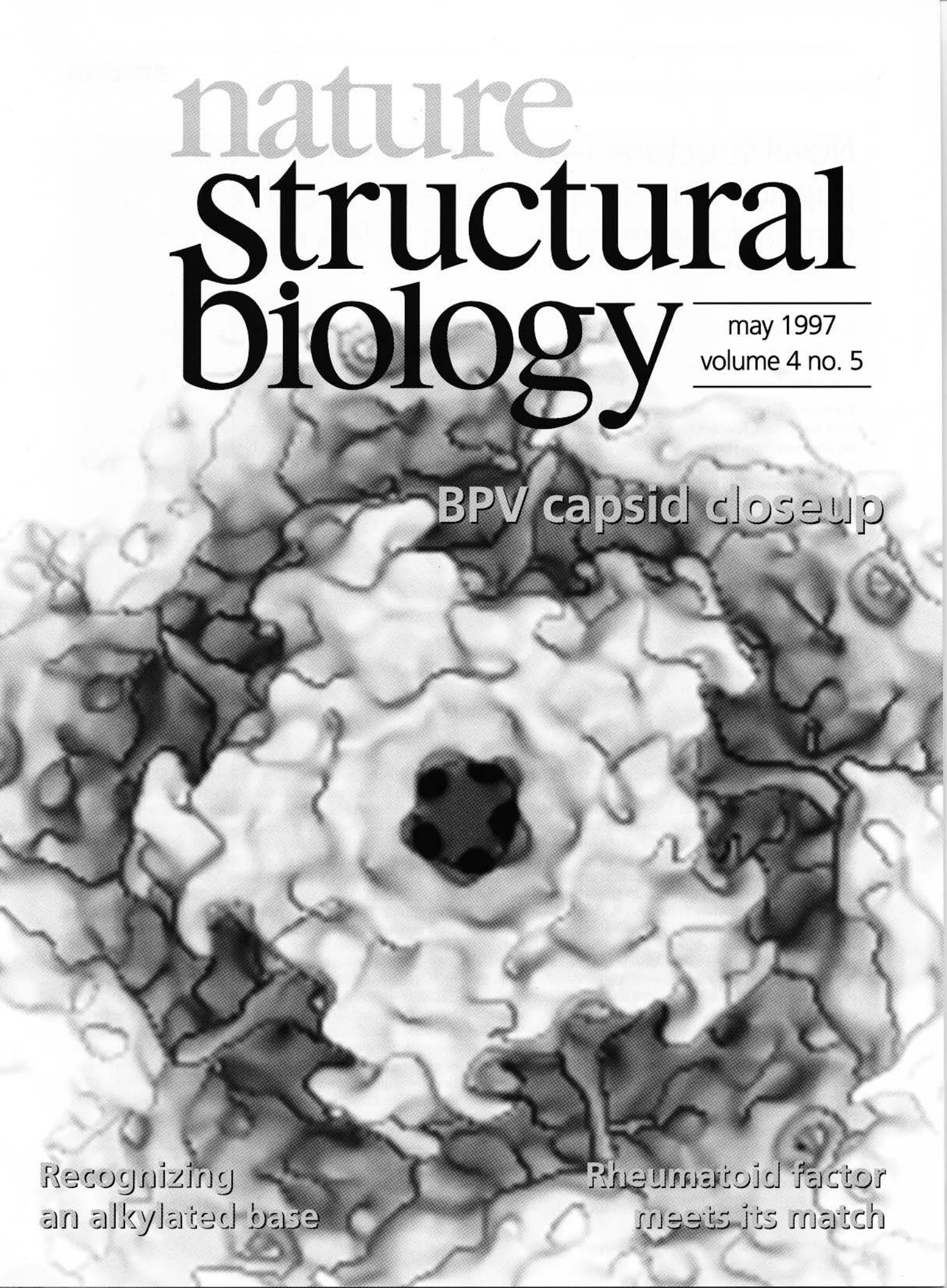

BPV capsid closeup

Recognizing an alkylated base

Rheumatoid factor meets its match

Novel structural features of bovine papillomavirus capsid revealed by a three-dimensional reconstruction to 9 Å resolution

Benes L. Trus[1,3], Richard B.S. Roden[2], Heather L. Greenstone[2], Michael Vrhel[4], John T. Schiller[2], and Frank P. Booy[3]

The three-dimensional structure of bovine papillomavirus has been determined to 9 Å resolution by reconstruction of high resolution, low dose cryo-electron micrographs of quench-frozen virions. Although hexavalent and pentavalent capsomeres form star-shaped pentamers of the major capsid protein L1, they have distinct high-resolution structures. Most prominently, a 25 Å hole in the centre of hexavalent capsomeres is occluded in the pentavalent capsomeres. This raises the possibility that the L2 minor capsid protein is located in the centre of the pentavalent capsomeres. Inter-capsomere connections ~10 Å in diameter were clearly resolved. These link adjacent capsomeres and are reminiscent of the helical connections that stabilize polyomavirus.

Papillomaviruses are epitheliatropic viruses of considerable medical interest. In addition to inducing benign proliferations (warts) in the epidermis and mucosal epithelium, infection by certain mucosatropic human papillomavirus (HPV) types is by far the most significant risk factor in the development of cervical cancer, the second most common cause of cancer deaths in women worldwide[1]. The development of prophylactic vaccines and therapeutics directed against papillomavirus virions may be furthered by an increased understanding of the virion structure, especially the location of antigenic and cell surface receptor binding sites.

Although not genetically related, papillomaviruses and polyomaviruses are grouped in the genus Papovaviruses because they have several common features including circular DNA genomes and non-enveloped icosahedral capsids with a T-number of 7, consisting of 72 pentameric capsomeres[2]. The structures of two similar polyomaviruses, simian virus 40 (SV40) and murine polyomavirus have been determined to near atomic resolution by X-ray diffraction[3–5]. No X-ray diffraction data are yet available for a papillomavirus because of the difficulty in purifying enough virions for crystallization trials. However, a sufficient quantity of virions for cryo-electron microscopy can be readily purified from warts for some papillomavirus types[6,7].

Since the pioneering work of Unwin and Henderson in low-dose electron microscopy applied to biological specimens[8] and the commercial availability of more stable low-temperature specimen cooling holders, electron crystallography has become a well established means for determining the structure of two-dimensional membrane protein crystals at atomic resolution (see, for example, Henderson *et al.*[9] and Kühlbrandt and Wang[10]). For non-crystalline specimens, even those possessing a high degree of symmetry, progress towards high resolution has been slower. The absence of electron diffraction data makes it less certain that structures are indeed preserved to high resolution and there is no direct access to structure factor amplitudes unattenuated by imaging defects[11]. Nonetheless, with well ordered helical polymers, Unwin was able to analyse the acetylcholine receptor to 9 Å resolution[12] and Jeng *et al.* visualized tobacco mosaic virus at 10 Å resolution[13]. Using programs originating with the 'common lines' procedures[14], the structures of several viruses have been determined to modest resolution (25–40 Å; see, for example, refs 15, 16). In 1995 herpes simplex virus capsids were visualized at 20 Å (ref. 17) and using newer algorithms, significant advances have been reported with reconstructions at 19 Å, 17 Å and 15 Å resolution[18–20].

The three-dimensional structures of bovine papillomavirus type 1 (BPV1), human papillomavirus type 1 (HPV1) and cottontail rabbit papillomavirus (CRPV) have been solved to moderate resolution (25–30 Å) and closely resemble each other[6,7]. The capsid shell of papillomaviruses contains the major, L1, and minor, L2, capsid proteins in a molar ratio estimated at approximately 30:1 (refs. 21, 22). L1 forms pentamers and self assembles into virus-like particles (VLPs), even in the absence of L2[23]. VLPs purified from cells driven to over-express HPV1 L1 from recombinant vaccinia were reconstructed and shown to have a very similar capsid structure to virions, demonstrating that L1 forms the capsomeres[24,25]. L1 co-assembles with L2 into VLPs[26] and both capsid proteins are required to generate infectious virus[22,27]. However, no difference in structure was found between HPV1 L1 only or L1/L2 VLPs at a resolution of 35 Å, so the location of L2 in the capsid remains to be determined[25]. The ability of an antibody to L2 to neutralize papillomavirus infectivity demonstrates that a portion of the protein is exposed on the surface of the capsid[28,29]. In addition, the requirement of L2 for genome encapsidation[22,27] and its ability to bind DNA non-specifically *in vitro*[30] suggest that L2 also is in contact with the genome, at least during packaging. No

[1]Computational Bioscience and Engineering Laboratory, Division of Computer Research and Technology [2]Laboratory of Cellular Oncology, National Cancer Institute, [3]Laboratory of Structural Biology, National Institute of Arthritis, Musculoskeletal and Skin Diseases, [4]Biomedical Engineering and Instrumentation Program, National Center for Research Resources, National Institutes of Health, Bethesda, Maryland 20892–5624, USA

Correspondence should be addressed to B.L.T. *trus@ipalph.dcrt.nih.gov*

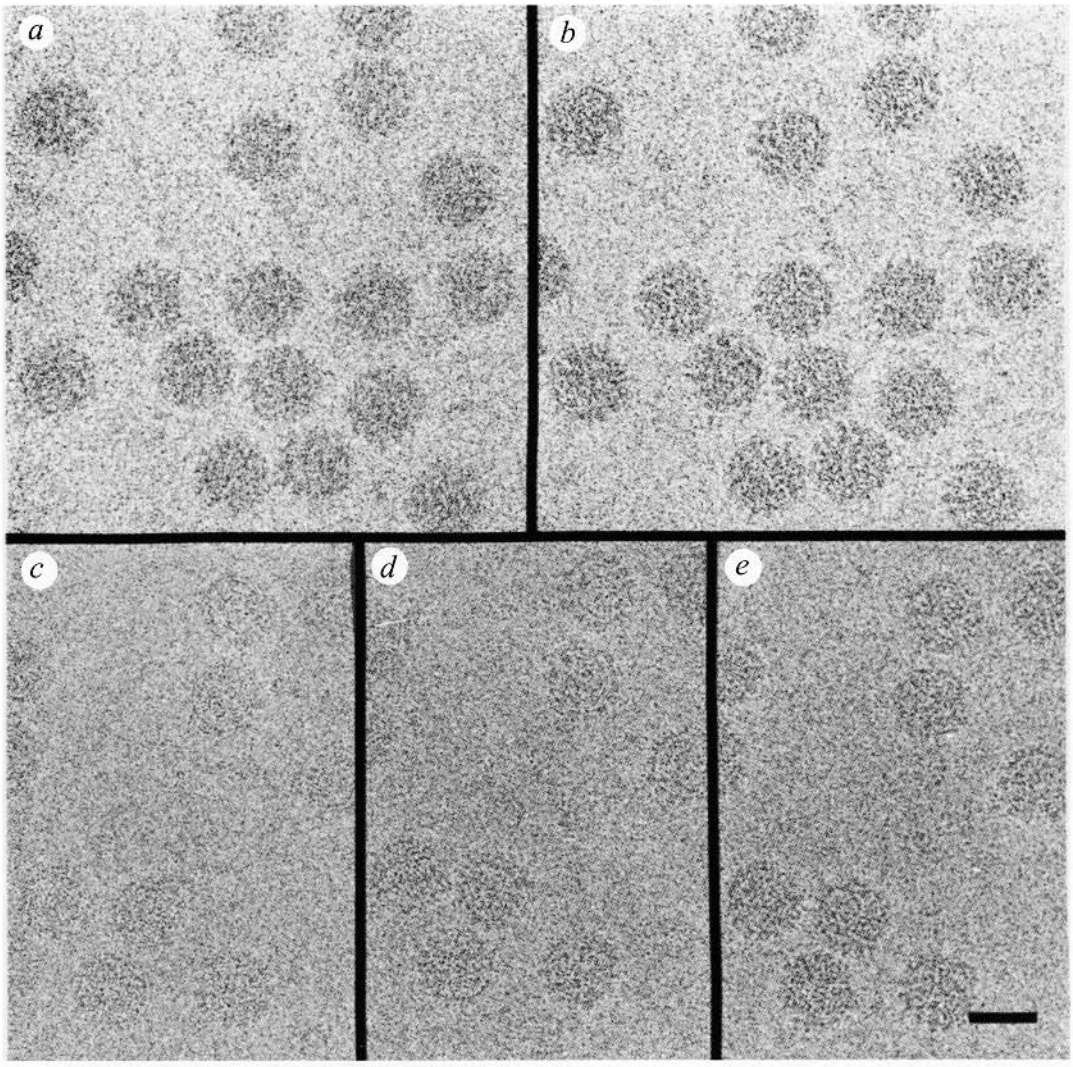

Fig. 1 *a,b*, A region of a pair of electron micrographs from the EM 400 with the first zero in the contrast transfer function (CTF) at 13 Å and 21 Å respectively. *c–e*, A region of a triplet from the CM20 microscope with the first zero in the CTF at 19 Å, 23 Å and 26 Å. Bar= 500 Å.

ordered structure has been observed for the 8 kbp double-stranded and histone-bound circular DNA of the papillomavirus genome, but there is evidence for contact with the capsid[2,6].

Here we report the structure of BPV1 virions at 9 Å resolution. This represents a major advance towards atomic resolution. Previously, such high-resolution data were only available from crystallographic studies. This advance results from combining a series of electron micrographs recorded at different defocus values, incorporating a correction for the contrast transfer function of the electron microscope, correcting for minor magnification variation across the micrograph and improvement of the reconstruction software. The capsomere structure and inter-capsomere contacts determined for a papillomavirus, using this modified reconstruction protocol, were compared to those previously calculated for other papovaviruses using X-ray diffraction analyses.

Capsid structure

The icosahedral nature of the virions and capsomere protrusions were readily apparent in low-dose cryo-electron micrographs of native virions (Fig. 1). Fig. 1*a,b* shows a region of a defocus pair of electron micrographs from the Philips EM400RT electron microscope and Fig. 1*c–e* shows a region of a focal triplet from the Philips CM20 electron microscope. The first zero in the contrast transfer function (CTF) was determined to be 13 Å and 21 Å for Fig. 1*a,b*, and 19 Å, 23 Å , and 26 Å for Fig.1 *c,d* and *e*. Two other CM20 defocus pairs were used in the calculation of the 12 Å reconstructions with their first zero in the CTF at 20 Å, 23 Å, and 21 Å, 25 Å. These four micrographs were not included in the 9 Å reconstruction because their contribution of signal at 9 Å was minimal. The lower contrast in CM20 images results, in part, from the higher acceleration voltage used and caused us to analyse micrographs recorded further from focus in order to visualize the BPV capsids by eye.

The data from the EM400 and CM20 were analysed separately. The results obtained were similar, but the EM400 results were slightly noisier (data not shown). The final reconstruction at 12 Å contains 581 images that were derived from only the CM20 . This is shown viewed down a five-fold axis of symmetry (Fig. 2). In the progression from 18–12 Å (Fig. 2*a–c*), the lower resolution reconstructions are simply the higher resolution result band limited (high frequencies removed). The capsid is shown as the dextro enantiomer[7] (Fig. 3*a*). Overall, the reconstruction shows similar features to the previously published data[6] although some clear differences can be seen. For example, the skewing noted in serial sections by Baker *et al.*[6] can be seen directly modulating the star shaped capsomeres in the surface shaded views even at 18 Å. However, as the resolution improves, finer features are resolved and differences are readily apparent between the two types of capsomere.

For example, clear holes are seen in the centre of hexavalent capsomeres, but not pentavalent capsomeres (Figs 3,4).

Fig 4 shows a comparison of the close-up view of the pentavalent and hexavalent capsomeres visualized at 12 Å resolution. The ~25 Å hole in the centre of the hexavalent capsomeres is clearly occluded in the pentavalent capsomere. Surface shaded cutaway and central density sectional views (Fig. 5) of the two types of capsomeres reveal the differences in the shapes of their internal cavities and further illustrate the extent of occlusion of the channel in the centre of the pentavalent capsomere.

The holes in the capsid shell previously reported to be ~5 Å in diameter[6] appear larger at higher resolution, with contouring at 110% of mass. We measure the hole on the two-fold axis to be rectangular, ~18×12 Å and the adjacent hole to be about half that size. Both the previous reconstruction and the present results analysed BPV in the closed form[7].

Inter capsomere links

A subset of 209 images from three CM20 micrographs (Fig. 1*c–e*) was used to calculate a reconstruction at 9 Å. These results are more easily visualized by examining a smaller volume of data or by looking at serial sections or stereo pairs. A surface close-up view of the pentavalent capsomere in stereo is shown (Fig. 3*b*) at 9 Å resolution, the limit of this analysis. Note the clear visibility of protien protrusions emanating from the facets of the pentavalent capsomeres and extending towards a vertex of each of the five neighboring hexavalent capsomeres. These connections, which are centred in sections ~16 Å above the top of the floor region (the region of continuous spherical protien density) and are apparently not directly linked to the floor, are reminiscent of the C-terminal connections observed in polyomavirus[5]. A section through the pentavalent capsomere of papillomavirus is shown (Fig. 6*a*). Pairs of arms are also visible connecting adjacent hexavalent capsomeres. By comparison, a section that displays the intercapsomerelinkage in ployomavirus at 9 Å resolution is shown (Fig. 6*b*). Close to the floor, linkages are also seen between pentavalent and hexavalent capsomeres. However, in contrast to papillomavirus, only a single link between hexavalent capsomeres is seen.

Links to the DNA core

Is the protein capsid connected to the nucleohistone core? Direct connections between the capsid shell and the enclosed nucleohistone core were investigated using the program UNBLOB[31] which removes disconnected density at a chosen threshold level. No linkages were seen at 15 Å or lower resolution. However, at 12 Å resolution, the nucleohistone core was not removed by this algorithm implying that there are thin linkages present. These connections directly link the floor region to the core, below the walls of the hexavalent capsomere protrusions and between the capsomeres (data not shown). No connections were visible below the hollow conical capsomere protrusions nor at all in the vicinity of the five-fold capsomeres. It is surprising that in an earlier papillomavirus reconstruction[6], which did not have a CTF correction, similar connectivity was also observed (underfocussed images without a CTF correction may exaggerate boundaries such as those between protein and DNA).

Capsomere structure

The basic structure of the virus as reported previously[6] is confirmed by the results shown in Fig. 2. However, with the improved resolution it is possible to see the features in considerably more detail. There are several differences between the two types of capsomeres. Most striking is the ~25 Å hole in the centre of the hexa-

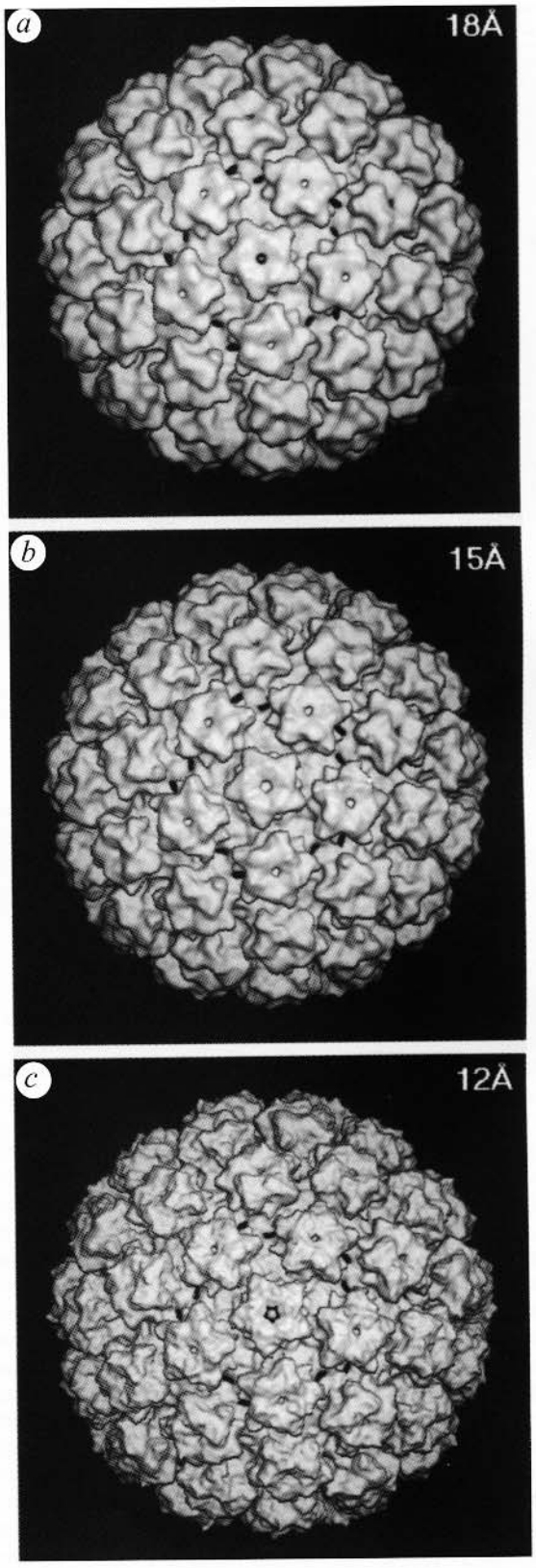

Fig. 2 A three-dimensional reconstruction from 581 CM20 images from three focal series derived from seven micrographs is visualized down the five-fold axis at *a*, 18 Å, *b*, 15 Å and *c*, 12 Å resolution. Disconnected density has been removed, and for the 12 Å image the connected DNA has been computationally removed. The lower resolution images (*a*,*b*) were calculated by band-limiting the data in the 12 Å reconstruction.

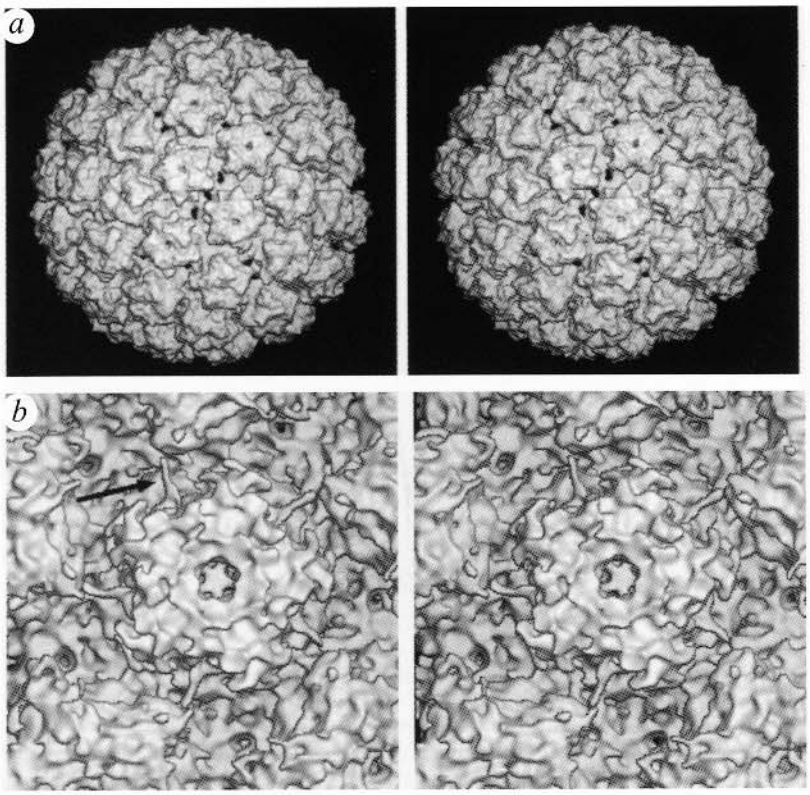

Fig. 3 *a*, A stereo view of BPV virus visualized at 12 Å down the two-fold axis of symmetry. *b*, A stereo close-up of BPV virus visualized at 9 Å resolution down the pentavalent capsomere. 209 images were used in the 9 Å reconstruction. Helical connections between capsomeres are visualized (arrow).

valent capsomeres; in the pentavalent capsomere the hole is weakly occluded close to the distal tip for ~30 Å, then solidly blocked (Figs 3*b*, 4, 5) for a short distance about half-way down the capsomere. In cross-section both capsomeres have the characteristic 'pointed star' shape previously described[6]. Both types of capsomeres have a twist associated with them. In the 12 Å reconstruction this twist is most prominent in the narrower portion ~20 Å above the floor where the points of the star appear abruptly rotated by ~36°. It is from close to these points that the more distal capsomere linkages originate. The sides of the pentavalent capsomere appear somewhat flatter and smoother, almost faceted, from this point to the distal tips, with only a small (~5°) rotation a few Ångstroms from the distal tip. The majority of the nodules of protruding density are approximately aligned under the points of the star.

In contrast, on the hexavalent capsomeres, the nodules of density protrude in different radial directions giving the impression of a more layered structure with a significant twist occurring ~25 Å from the floor rather than the continuous twist noted at lower resolution[6]. This was most clearly seen in distal radial sections of the capsomeres (data not shown).

Papillomavirus and Polyomavirus: a comparison

All Papovaviruses studied to date have T=7 icosahedral symmetry derived from 72 pentameric capsomeres. Papillomavirus, with a diameter of 600 Å, is ~100 Å larger in diameter than polyomavirus. This size difference is due largely to the L1 protein chain of BPV1 being 111 residues longer than the major capsid protein, VP1, of polyomavirus. There is little sequence similarity between the papillomavirus L1 and VP1 of polyomavirus[7]. While both polyomavirus and SV40 have been crystallized and their X-ray structures are known, this is the first reported high-resolution EM structure of papillomavirus that can be utilized to compare structural motifs in detail. The structures of polyomavirus and SV40 are similar, so the coordinates of only polyomavirus have been utilized to generate a three-dimensional map at 8.5 Å resolution to compare with our results for papillomavirus.

The most interesting similarity between our reconstruction of BPV1 and polyomavirus is the inter-capsomere linkages seen connecting the pentavalent capsomere to each surrounding hexavalent capsomere ~16 Å above the outer shell surface (Fig. 6). In each case, these connections are ~10 Å in diameter. However, the angle with which these inter-capsomere linkages approach the pentavalent capsomeres differs by about 45°, such that the linkage appears longer in polyomavirus. BPV and polyomavirus appear to differ substantially in inter-hexavalent capsomere linkages. While adjacent hexavalent capsomeres in murine polyomavirus and SV40 are linked by a single crossbridge[3,5] adjacent hexavalent capsomeres in BPV have two distinct crossbridges. These linkages are at the resolution limit of our CM20 data and a higher resolution analysis would be required to more clearly understand the details of these structures. The three-dimensional reconstruction using the CM20 data shows this linkage more clearly, at least in part, because of the improved CTF provided by the higher coherence of the field emission gun.

As pointed out by Baker[6], a major difference between capsomeres of papillomavirus and polyomavirus is that papillomavirus capsomeres are star shaped and slightly wider at the top, whereas polyomavirus capsomeres are much more rounded and conical in shape. This difference was attributed to the extra mass of L1, noted above, contributing to the wider top, as can be seen in both the stereo images (Fig. 3). The lack of sequence similarity between L1 and VP1 prevents localization of the additional mass of L1 as, for example, being attributed to a single bump or lump in the papillomavirus reconstruction. For the same reason, we cannot reliably say which ~110 amino acids in the sequence correspond to the additional mass in L1.

It is noteworthy that the papillomavirus hexavalent capsomeres do not extend outward normal to the spherical shell, but are tilted a few degrees (Fig 5). The hexavalent capsomeres in polyomavirus, but not SV40, were also observed to be tilted off-axis by 2.6° (ref. 5).

Location of L2

Papillomaviruses and polyomaviruses contain a different number of capsid proteins. Polyomavirus is composed of 360 copies of its major capsid protein, VP1, that can similarly self assemble into VLPs[2,16,32]. In addition, there are 72 copies of a minor capsid protein (VP2 or VP3), with one per capsomere[33]. VP1 forms conical capsomeres and the partially disordered density inside these hollow cones is attributed to internal VP2 or VP3[3,33]. Papillomavirus is composed of a major capsid protein (L1) and an unrelated minor capsid protein (L2). There are 360 copies of L1 per virion or five per capsomere[2]. At low resolution (~35 Å) VLPs made from HPV1 L1 alone appeared identical to the L1 plus L2 VLPs[25]

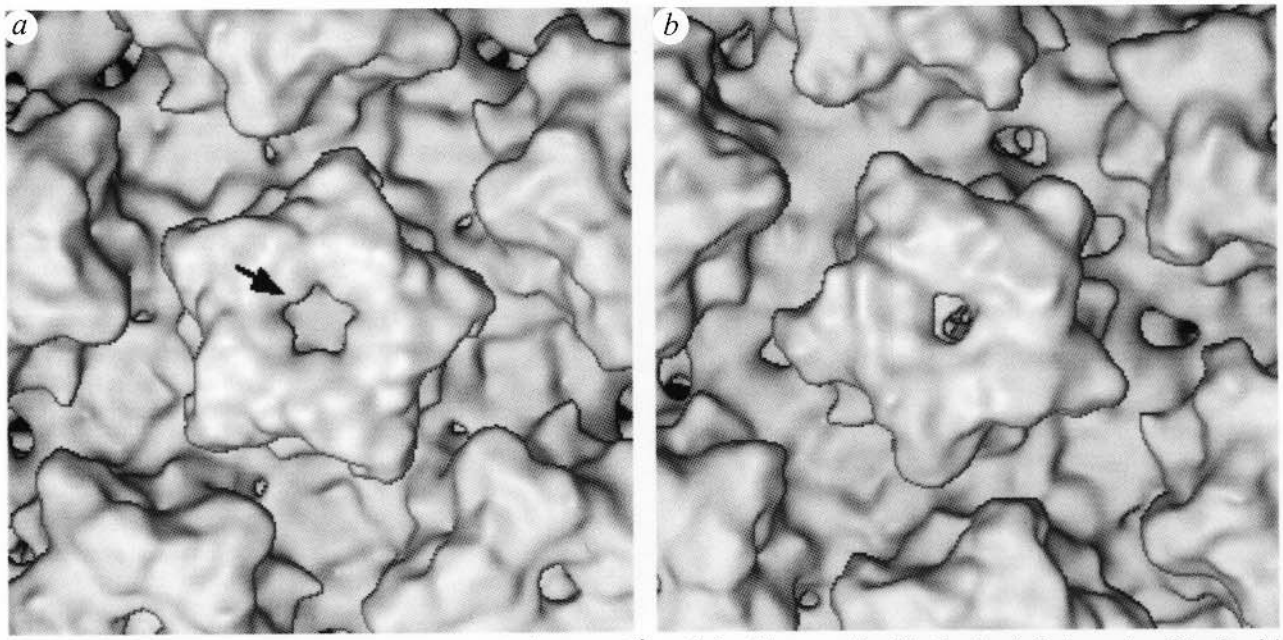

Fig. 4. *a*, A close-up view of the pentavalent capsomere is shown at 12 Å resolution. The arrow identifies the density in the centre of the five-fold capsomere that may be the minor capsid protein L2. *b*, The hexavalent capsomere is shown at 12 Å resolution for comparison.

demonstrating that L1 forms the majority of the capsid shell. Estimates for the number of copies of L2 have varied from ~36 (ref. 34), to most recently only 12 (refs. 21, 22). These estimates were made by densitometry of L1 and L2 bands on SDS-PAGE gels of BPV virions stained with Coomassie blue.

If there are just 12 copies of L2 in papillomavirus, only a few possibilities exist for its location: (i) L2 could be associated with a single (portal) capsomere or a very few capsomeres; (ii) L2 has an internal function and its location on the surface lattice is not important so it is distributed randomly among 12 of the 72 capsomeres or it could be accessible through the holes in the capsid shell structure; (iii) the 12 L2 molecules could be associated with 12 distinct capsomeres such as the pentavalent capsomeres. If L2 were associated with one (or a very few) capsomeres, such as a portal capsomere in bacteriophages, or randomly distributed among the capsomeres, then there would be insufficient signal to distinguish L1 capsomeres from L1/L2 capsomeres after icosahedral reconstruction. Therefore, the shape and cross section of the two types of capsomeres would be expected to be similar, provided that differences in the local bonding environment do not markedly influence the shape of the capsomere. This is not observed in our reconstruction of BPV1. Furthermore, immunogold labelling experiments of L2 in HPV1-derived L1/L2 VLPs do not support the existence of an L2-portal vertex[24]. If L2 were associated with just the twelve pentavalent capsomeres, then these capsomeres may be expected to appear somewhat different from the hexavalent capsomeres at higher resolution and some density should be seen corresponding to the location of the L2. In fact, if one compares the pentavalent and hexavalent capsomere, distinct differences are seen. In cross section, the internal shape of each capsomere is different. The pentavalent capsomere has a slightly wider base whereas the hexavalent capsomere is essentially parallel-sided but tilted (Fig. 5). There is some density in the centre of the pentavalent capsomeres occluding the ~25 Å hole (Fig. 5*a*),

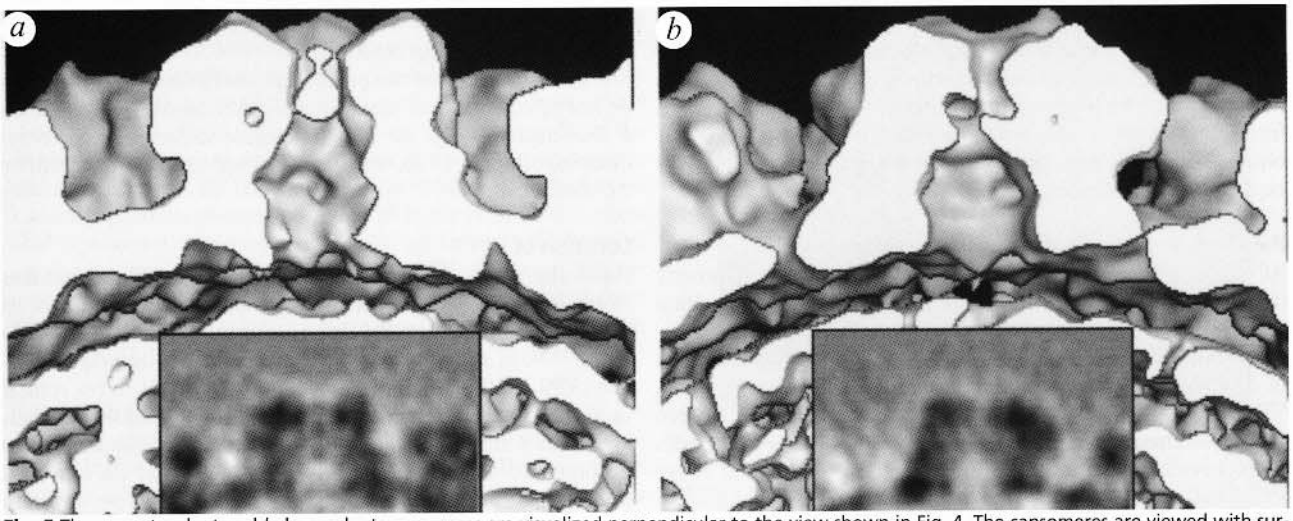

Fig. 5 The *a*, pentavalent and *b*, hexavalent capsomeres are visualized perpendicular to the view shown in Fig. 4. The capsomeres are viewed with surface shading but with the front half of the capsomere removed. The central density section is reduced in size by one half (inserts) from the surface shaded view, and protein is visualized in black.

which is absent in the hexavalent capsomeres (Fig. 5*b*). This density may be L2. Although the mass of this density is insufficient to represent the entire L2 protein, it could be the portion of L2 that is icosahedrally ordered. Similarly, not all of the putative VP2/VP3 density was observed in SV40[3] or polyomavirus[5]. At the present time we cannot conclusively establish that this density is the L2 protein. We cannot, for example, rule out the possibility that the differences observed in the shapes of the pentavalent and hexavalent capsomeres are due primarily to the different environments of the two capsomeres. However, such a difference in environment does not produce a different conformation of VP1 for polyomavirus[5] or SV40[3].

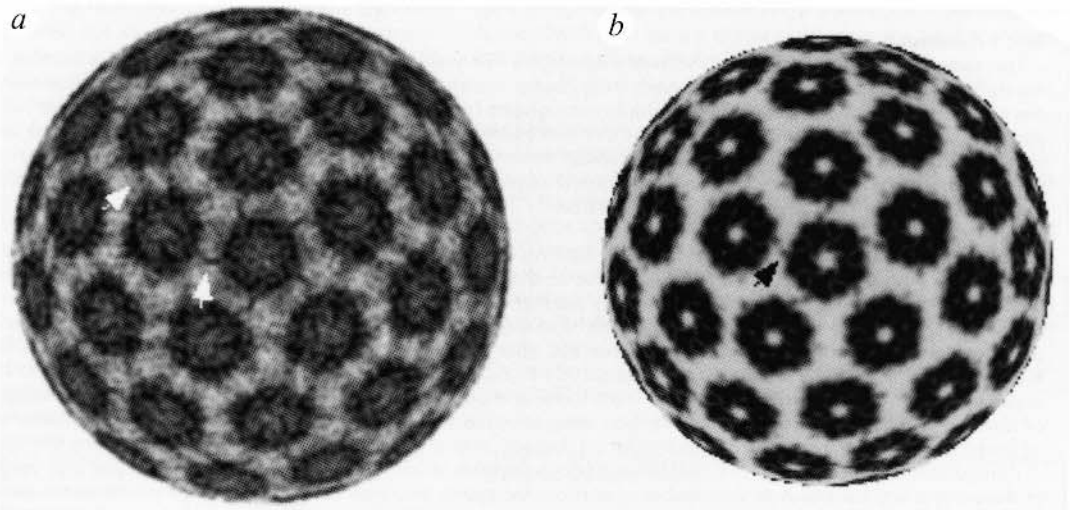

Fig. 6. A comparison of cross sections of the pentavalent capsomeres and their immediate hexavalent neighbours of *a*, papillomavirus visualized at 9 Å *versus b*, polyomavirus at comparable resolution[5]. The helical crosslinks (arrow) in polyomavirus may be compared with similar crosslinks in papillomavirus (arrows). The sections are visualized ~16 Å above the top of the floor region. Sections are 2.7 Å and 2.5 Å thick for papillomavirus and polyomavirus, respectively. The section (Fig. 6*b*) was calculated from atomic coordinates[5] using the program X-PLOR[56] and so are noise-free.

Neutralization studies of BPV1 with polyclonal antisera to L2 peptides suggest that a small region near the N terminus of L2 is accessible from the outside but the majority of the protein is inside the particle[28]. However, a three-dimensional reconstruction of BPV1 labelled with a neutralizing polyclonal antiserum to L2 did not resolve the antibody. A direct comparison of L1 alone and L1/L2 VLPs may be conclusive, but, to date, L1 alone VLPs have proven difficult to reconstruct to high resolution due to their heterogeneity in size and shape and previous attempts by others have been unsuccessful[25]. Nevertheless, a location of L2 in the centre of pentavalent capsomeres is most consistent with the present data.

In vitro non-specific DNA binding and the requirement for L2 in encapsidation suggest that L2 also contacts the nucleohistone core[22,27,30]. An association of the L2 molecule with the non-icosahedral nucleohistone core would be likely to blur the binding domain of L2 during the application of icosahedral symmetry in the reconstruction process. This may explain why insufficient density to account for L2 was observed in the button inside the pentavalent capsomeres. It is interesting to speculate that the 12 pentavalent capsomeres may in fact be somewhat similar in structure to all capsomeres in polyomavirus or SV40 with a disordered internal protein in a conical cavity[3,33]. The connections observed in this study between the capsid and the DNA-containing core are similar to previous observations[6] and are not under the pentavalent capsomeres, but between hexavalent capsomeres, and therefore are unlikely to involve L2, assuming it is located in the pentavalent capsomeres.

Do the hexavalent capsomeres have five-fold symmetry?

Those capsomeres that do not lie on a symmetry axis are not required to be symmetric. For example, the peripentonal capsomeres in the procapsid of herpes simplex virus are elliptical[35] and the hexons in the procapsid for Hong Kong 97 are sheared[36]. As visualized in Fig. 3*a*, the hexavalent capsomere shows almost perfect five-fold symmetry. It is our opinion that the hexavalent capsomere, while in an asymmetric environment, is rather symmetrical and that the slight asymmetry would disappear (i) at higher resolution and (ii) as substantially more images were added to the three-dimensional reconstruction. This is based on our observation that the asymmetric capsomere has become more symmetrical as more images were included in the reconstruction. In fact, if we calculate the degree of asymmetry for the hexavalent capsomere for a section ~25 Å from the tip, the capsomere is ~95% symmetric. This is based on calculating the total power or variance of one section *versus* the total power of the same section to which five-fold symmetry has been imposed.

Box 1

Resolution assessment We determined the resolution of our reconstruction by three independent methods. We used traditional resolution assessment techniques[37], our own previously published protocol (FRC3D)[38], and a new improved three-dimensional SSNR method[39]. All three criteria indicated that the resolution obtained was 9 Å. In the inverse eigenvalue spectrum, 99.4% of the eigenvalues are <0.001. In addition to these statistical resolution estimates, direct observations of the data also support 9 Å resolution. The three-dimensional reconstruction clearly shows connections between the capsomeres that are not resolved above 9 Å and are very similar to the helical connections seen in polyomavirus. A detailed explanation of our resolution assessment is provided in supplementary material available from the authors (see *http://cbel.dcrt.nih.gov/ntrus/nsb97/html*).

The first requirement for attaining 9 Å resolution is that the micrographs contain data to the desired resolution. An analysis of the extent of the Thon rings from the electron micrograph on an optical bench will quickly assess the resolution to which the microscope was performing. For the data presented here, the Thon rings extended to 8.0 Å in the EM 400 micrographs and 6.0 Å in the CM20 micrographs. Whether or not individual virions are imaged to this resolution depends on many other factors (for example, electron dose, signal-to-noise ratio (S/N), contrast) and can only be determined by a full structural analysis. The CM20 data used here had an improved S/N ratio at high resolution compared with the EM 400 data. During subsequent analysis, the quality of the data must be preserved at each step. For example, use of a very accurate densitometer is required to prevent loss of resolution in the digitization step[40] (see Methods).

Box 1 continued next page

Box 1 continued

Our data were preprocessed using software developed in-house (X3DPREPROCESS) which provides a number of reported improvements[38]. In our experience, the use of Baker's Polar Fourier Transform (PFT) Program[41,42] for refinement has proven far superior to previous cross-common line refinement[15,16]. Multiple micrographs from a focal series must be combined accurately not only to preserve, but also to enhance the information content of the individual images[43]. For the CM20 data, for example, the correlation coefficients obtained from PFT on combined images were about three times greater than the correlation coefficients obtained from single images. Careful assessment and correction of magnification changes across the field of a micrograph are required[44]. Finally, accurate determination of the resolution of the reconstruction is essential[39].

Resolution limits Several factors are presently limiting our ability to achieve higher resolution. The specimen cooling holder used to collect data on the EM400 is limiting at ~8 Å due to the vibrations of the boiling liquid nitrogen and damping inadequacies of the goniometer stage of the EM[45]. Additionally, stray magnetic fields around the EM limit the CTF to ~8 Å. The cooling holder used on the CM20 becomes limiting at ~6.5 Å due to its sensitivity to acoustic noise, but the CTF of the EM is not limiting at this point. The S/N ratio of the micrographs is limiting with micrographs recorded close to focus under the present experimental conditions. With the present data, it was not possible to easily locate or determine particle-orientations for images with the first zero in the CTF below ~20 Å. The S/N ratio is improved by recording micrographs further from focus, and potentially by recording data without a carbon supporting film (by the use of holey carbon films), by increasing the electron dose, or by reducing the accelerating voltage used. The disadvantages are increased risk of limitation due to charging[46], increased radiation damage, and increased multiple and dynamic scattering effects.

Computationally, the noise in the final reconstruction depends to a large extent on the number of particles used in the reconstruction. In this study it was clear that as the number of particles increased, the noise was reduced, and the hexavalent capsomeres became more symmetrical. Precisely how to determine the minimum number of particles required to reach a specific resolution is not known, although some estimates have been made[47]. The software that has been developed should be capable of producing structures to significantly higher resolution. While future refinements in algorithms will strive to extract more signal from low-contrast images, some accommodation can be achieved by combining more images in the reconstruction process.

Since radiation damage has not been limiting for electron crystallography studies to atomic resolution, it seems reasonable to suppose that similar higher resolution data could be collected and analysed for icosahedral particles. The resolution that will be required to resolve the β-barrel structure that is expected to form the papillomavirus capsomeres is presently unclear, but in the case of X-ray crystallography, under optimal conditions a resolution of 6 Å may be sufficient (M. Rossman, personal communication). While many more particles will be required in such an analysis, it seems that resolution of such structures by these techniques should be possible.

Methods

Purification of BPV. Bovine warts (a gift from C. Olson) were washed in phosphate-buffered saline (PBS) and cut into small pieces. Approximately 150–200g of wart was homogenized with 400 ml of ice cold PBS containing 0.5M NaCl (PBSS) in a Waring blender (3×2 min. with cooling periods between homogenization). The wart extract was centrifuged (20 min., 10,000 g, 4 °C), the pellets re-extracted, and the supernatants combined. The BPV was harvested from the supernatant by centrifugation (1h, 140,000 g, 4 °C), resuspended by sonication in 33% (w/w) CsCl in PBS and purified by isopycnic density gradient centrifugation (20h, 300,000 g, 10 °C). The band containing BPV was harvested, dialysed against PBSS, and loaded on to a 10 ml 40% (w/v) sucrose in PBSS cushion in a Beckman SW-40 rotor. The BPV was centrifuged through the cushion (150 min., 120,000 g, 4 °C), resuspended in 200 µl and dialysed exhaustively against PBSS at 4 °C.

Cryo-electron microscopy. Drops of BPV at ~1 mg ml^{-1} in PBS were placed on carbon-coated 400 mesh Cu EM grids (freshly washed in the vapour of refluxing acetone), reduced to a thin film by blotting and quench-frozen in liquid ethane using a KF 80 (Reichert) as described previously[48]. Micrographs were initially recorded using low-dose procedures on a Philips EM400RT equipped with a modified, second series, type 626 Gatan cooling holder and modified Gatan anti-contamination blades. The microscope was operated at 100 KV with the C1 lens highly excited and 20 µA emission from a LaB_6 tip and images were recorded at 46,000 ×, with a dose of ~11 eÅ^{-2} per micrograph, on Kodak SO 163 emulsion developed for 15–18 minutes in D19. Subsequently, additional micrographs were recorded on a Philips CM20 FEG microscope operating at 200 KV and 38,000× with a third series Gatan 626 cooling holder using Agfa 23D56 emulsion developed for eight minutes in D19 with a dose of ~5 e Å^{-2} per micrograph. Micrographs were recorded as defocus pairs on the EM 400 and defocus triplets on the CM20. The closest to focus micrograph was recorded first in each case. Micrographs were initially screened by optical diffraction to assess stigmation and defocus and by eye for appropriate numbers of particles, ice thickness, and contrast.

Image processing and three-dimensional reconstruction. The selected micrographs were digitized on a Perkin-Elmer 1010MG microdensitometer at a sampling rate of ~3 Å per pixel. Images were preprocessed using X3DPREPROCESS[38]. Originally, reconstructions were calculated by 'common lines' techniques of Fourier Analysis[14–16] as described[49,50]. The computationally intensive programs used to estimate and then refine the particle's orientations were adapted from code kindly given to us by T.S.Baker (Purdue University) and extensively modified to run on an Intel iPSC/860 Supercomputer[51,52]. Once a satisfactory low resolution model was obtained, the orientational parameters were refined to higher resolution by the Polar Fourier Transform method (PFT)[41,42]. Cross-common line refinement, while satisfactory to about 20–25 Å resolution, has been a significant impediment to achieving high resolution.

Magnification was corrected[44] across micrographs using a modified Marquardt–Levenberg optimization[53]. Magnification varied by up to 2% across the field of view[54]. Typically, greater magnification was observed toward the centre of the electron micrographs, with a smooth radial decrease. A 2% error in magnification would blur capsids by ~6 Å at the outer radius. While correction of this distortion is not significant for traditional three-dimensional reconstructions, it is required for high resolution.

Initially, the structure was solved and refined up to the first zero in the CTF using the further from focus image. For each set of micrographs, the CTF was corrected in two different ways. First, the phases in alternate zones of the CTF were simply flipped and the individual micrograph images were refined separately and subsequently combined in the three-dimensional reconstruction. Second, the images were combined using a more sophisticated CTF correction algorithm[43]. This procedure uses a multi-channel Wiener restoration technique. In this approach, a CTF model (based on the defocus and known microscope parameters) is first calculated. Noise statistics are then determined from background sections of the micrograph and a simple parametric first order Markov model is used to model the power spectrum of the underlying signal. From the CTF model and an estimate of the spectral signal-to-noise-ratio, a pair of filters may be computed that, given an image pair as input, maximizes the signal-to-noise ratio in an image that is the sum of the filter outputs. The same procedure could be applied to a defocus triplet. In implementing the procedure, the images in a focal series are first accurately aligned[44], then filtered with the appropriate Wiener filter, and then added together to obtain a single image. For the EM400RT focal pair, the improvement over separate images resulting from our CTF combination of the two images was determined to be ~25% based on Fourier ring correlation criteria[38]. Data were refined with simple flipping as well as with our improved CTF correction, and the FRC com-

pared for both data sets. The final reconstruction from the EM400RT data (not shown) contained 264 images combined into CTF corrected images; the final reconstruction from the CM20 contained 581 separate images to 12 Å and 209 separate images at 9 Å. Resolution (as described in box 1 see *http://cbel.dcrt.nih.gov/ntrus/nsb97/html*) was determined to be 9 Å for data from both the EM400 and the CM20.

Figures that highlight very high resolution (9 Å) details (Figs 3*b* and 6) use 209 separate CM20 images. Other figures, which show general structural features (to 12 Å) use 581 CM20 images. The threshold for surface shading was selected to view 110% of the expected mass[31]. This threshold is about two standard deviations above background. Three-dimensional EM reconstructions are usually shown with 100–120% of expected mass. This is because the simplistic approximation that all pixels contain the same mass density is not accurate and also because in our experience, 100% of mass tends to provide an artificially 'holey' or discontinuous structure. In our opinion, while the EM400RT data are statistically accurate to 9 Å, the CM20 data have a better signal-to-noise ratio for visualizing fine details such as ~10 Å helical connections.

Acknowledgements

We wish to acknowledge Alasdair Steven, Douglas Lowy and Robert Martino for encouragement and advice. We thank Carl Olson for his generous gift of bovine wart material. We would also like to thank Philippe Thévenaz and Michael Unser for magnification assessment and assistance with CTF corrections, David Belnap and James Conway for assistance in the use of X-PLOR and re-analysis of the X-ray structure of polyomavirus, Eva Kocsis for programming assistance, and Thilo Stehle for providing the polyomavirus X-ray atomic coordinates and helpful discussions. We are grateful to Tim Baker and Steve Fuller for making icosahedral software available to us and to Steve Fuller for helpful suggestions concerning resolution.

Received 21 November 1996; Accepted 7 March 1997

1. Lowy, D.R., Kirnbauer, R. & Schiller, J.T. Genital human papillomavirus infection. *Proc. Natl. Acad. Sci. USA* **91**, 2436–2440 (1994).
2. Baker, T.S. & Rayment, I. *Papoviridae* (Elsevier, 1987).
3. Liddington, R.C. *et al.* Structure of simian virus 40 at 3.8 Å resolution. *Nature* **354**, 278–284 (1991).
4. Stehle, T., Gamblin, S.J., Yan, Y. & Harrison, S.C. The structure of simian virus 40 refined at 3.1Å resolution. *Structure* **4**, 165–182 (1996).
5. Yan, Y., Stehle, T., Liddington, R.C., Zhao, H. & Harrison, S.C. Structure determination of simian virus 40 and murine polyomavirus by a combination of 30–fold and 5–fold electron-density averaging. *Structure* **4**, 157–164 (1996).
6. Baker, T.S. *et al.* Structures of bovine and human papillomaviruses. Analysis by cryoelectron microscopy and three-dimensional image reconstruction. *Biophys. J.* **60**, 1445–1456 (1991).
7. Belnap, D.M. *et al.* Conserved features in papillomavirus and polyomavirus capsids. *J. Mol. Biol.* **259**, 249–263 (1996).
8. Unwin, P.N.T. & Henderson, R. Molecular structure determination by electron microscopy of unstained crystalline specimens. *J. Mol. Biol* **94**, 425–440 (1975).
9. Henderson, R. *et al.* Model for the structure of bacteriorhodopsin based on high-resolution electron cryo-microscopy. *J. Mol. Biol* **213**, 899–929 (1990).
10. Kühlbrandt, W. & Wang, D.N. Three-dimensional structure of plant light-harvesting complex determined by electron crystallography. *Nature* **350**, 130–134 (1991).
11. Henderson, R. & Glaeser, R.M. Quantitative analysis of image contrast in electron micrographs of beam-sensitive crystals. *Ultramicroscopy* **16**, 139–150 (1985).
12. Unwin, N. Nicotinic acetylcholine receptor at 9Å resolution. *J. Mol. Biol* **229**, 1101–1124 (1993).
13. Jeng, T.-W., Crowther, R.A., Stubbs, G. & Chiu, W. Visualization of alpha-helices in Tobacco Mosaic Virus by cryo-electron microscopy. *J. Mol. Biol* 205, 251–257 (1989).
14. Crowther, R.A. Procedures for three-dimentional reconstruction of spherical viruses by Fourier synthesis from electron micrographs. *Phil Trans Roy Soc Lond B* **261**, 221–230 (1971).
15. Fuller, S.D. The T=4 envelope of Sindbis Virus is organized by interactions with a complementary T=3 capsid. *Cell* 48, 923–934 (1987).
16. Baker, T.S., Drak, J. & Bina, M. Reconstruction of three-dimensional structure of simian virus 40 and visualization of the chromatin core. *Proc. Natl. Acad. Sci. USA* **85**, 422–426 (1988).
17. Zhou, Z.H. *et al.* Assembly of VP26 in herpes simplex virus-1 inferred from structures of wild-type and recombinant capsids. *Nat. Struc. Biol.* **2**, 1026–1030 (1995).
18. Thuman-Commike, P.A. *et al.* Three-dimesional structure of scaffolding-containing phage P22 procapsids by electron cryo-microscopy. *J. Mol. Biol* 260, 85–98 (1996).
19. Zlotnick, A. *et al.* Dimorphism of Hepatitis B virus capsids is strongly influenced by the C-terminus of the capsid protein. *Biochemistry* **35**, 7412–7421 (1996).
20. Böttcher, B. & Crowther, R.A. Difference imaging reveals ordered regions of RNA in turnip yellow mosaic virus. *Structure* **4**, 165–182 (1996).
21. Volpers, C., Schirmacher, P., Streeck, R.E. & Sapp, M. Assembly of the major and the minor capsid protein of human papillomavirus type 33 into virus-like particles and tubular structures in insect cells. *Virology* **200**, 504–512 (1994).
22. Roden, R.B.S. *et al.* In vitro generation and type-specific neutralization of a human papillomavirus type 16 virion pseudotype. *J. Virol.* 70, 5875–5883 (1996).
23. Kirnbauer, R., Booy, F., Cheng, N., Lowy, D.R. & Schiller, J.T. Papillomavirus L1 major capsid protein self-assembles into virus-like particles that are highly immunogenic. *Proc. Natl. Acad. Sci. USA* **89**, 12180–12184 (1992).
24. Hagensee, M.E., Yaegashi, N. & Galloway, D.A. Self-assembly of human papillomavirus type 1 capsids by expression of the L1 protein alone or by coexpression of the L1 and L2 capsid proteins. *J Virol* **67**, 315–322 (1993).
25. Hagensee, M.E., Olson, N.H., Baker, T.S. & Galloway, D.A. Three-dimensional structure of vaccinia virus-produced human papillomavirus type 1 capsids. *J. Virol.* **68**, 4503–4505 (1994).
26. Kirnbauer, R. *et al.* Efficient self-assembly of human papillomavirus type 16 L1 and L1-L2 into virus-like particles. *J. Virol.* **67**, 6929–6936 (1993).
27. Zhou, J., Stenzel, D.J., Sun, X.Y. & Frazer, I.H. Synthesis and assembly of infectious bovine papillomavirus particles in vitro. *J. Gen. Virol.*, 763–768 (1993).
28. Roden, R.B.S. *et al.* Neutralization of bovine papillomavirus by antibodies to L1 and L2 capsid proteins. *J. Virol.* **68**, 7570–7574 (1994).
29. Gaukroger, J.M. *et al.* Vaccination of cattle with bovine papillomavirus type 4 L2 elicits the production of virus-neutralizing antibodies. *J. Gen. Virol.* **77**, 1577–1583 (1996).
30. Zhou, J., Sun, X.Y., Louis, K. & Frazer, I.H. Interaction of human papillomavirus (HPV) type 16 capsid proteins with HPV DNA requires an intact L2 N-terminal sequence. *J. Virol.* **68**, 619–625 (1994).
31. Conway, J.F., *et al.* Visualization of three-dimensional density maps reconstructed from cryoelectron micrographs of viral capsids. *J. Struct. Biol.* 116, 200–208 (1996).
32. Salunke, D.M., Caspar, D.L.D. & Garcea, R.L. Self-assembly of purified polyomavirus capsid protein , VP1. *Cell* **46**, 895–904 (1986).
33. Griffith, J.P., Griffith, D.L., Rayment, I., Murakami, W.T. & Caspar, D.L.D. Inside polyomavirus at 25Å resolution. *Nature* **355**, 652–654 (1992).
34. Doorbar, J. & Gallimore, P.H. Identification of proteins encoded by the L1 and L2 open reading frames of human papillomavirus 1a. *J. Virol.* **61**, 2793–2799 (1987).
35. Trus, B.L. *et al.* The herpes simplex virus procapsid: structure, conformational changes upon maturation, and roles of the triplex proteins VP19c and VP23 in assembly. *J. Mol. Biol.* **263**, 447–462 (1996).
36. Conway, J.F., Duda, R.L., Cheng, N., Hendrix, R.W., Steven, A.C. Proteolytic and conformational control of virus capsid maturation: The bacteriophage HK97 system. *J. Mol. Biol.* **253**, 86–99 (1995).
37. Saxton, W.O. & Baumeister, W. The correlation of averaging of a regularly arranged bacterial cell envelope protein. *J. Microscopy* 127, 127–138 (1982).
38. Conway, J.F. *et al.* The effects of radiation damage on the structure of frozen hydrated HSV-1 capsids. *J. Struct. Biol.* **111**, 222–233 (1993).
39. Unser, M. *et al.* Resolution Assessment of 3D Reconstruction by Spectral Signal-To-Noise Ratio. in 11th EUREM , Dublin, Ireland, 1996).
40. McGee, P.A., Trus, B.L. & Steven, A.C. Techniques to evaluate the performance of scanning microdensitometers in the digitization of electron micrographs. *Micron* **13**, 221–228 (1982).
41. Cheng, R.H. *et al.* Functional implications of quasi-equivalence in a T= 3 icosahedral animal virus established by cryo-electron microscopy and X-ray crystallography. *Structure* **2**, 271–282 (1994).
42. Baker, T.S. & Cheng, R.H. A model-based approach for determining orientations of biological macromolecules imaged by cryoelectron microscopy. *J. Struct. Biol.* **116**, 120–130 (1996).
43. Vrhel, M. & Trus, B.L. Multichannel Restoraton of Electron Micrographs. Proc. *IEEE Int. Conf. Image Proc.* 516–519 (B. Werner, ed., Washington, D.C., 1995).
44. Thévenaz, P., Ruttimann, U.E. & Unser, M. Iterative Multi-Scale Registration without Landmark. *Proc. IEEE Int. Conf. Image Proc* (B. Werner, Ed., Washington, D.C., 1995).
45. Booy, F.P. & van Bruggen, E.F.J.On the suitability of the available cooling holders for low-dose work with the Philips EM400. *Ultramicroscopy* **13**, 337–342 (1984).
46. Brink, J., Sherman, M., Berriman, J. & Chiu, W. Charging phenomena observed on biological specimens in a 400-KV electron cryo-microscope. in Proceedings Microscopy Society of America (eds Bailey, G.W. & Garratt-Reed, A.J.) 118–119 (San Francisco Press, New Orleans, 1994).
47. Henderson, R. The potential and limitations of neutrons, electrons and X-rays for atomic resolution microscopy of unstained biological molecules. *Q. Rev. Biophys.* **28**, 171–193 (1995).
48. Baker, T.S., Newcomb, W.W., Booy, F.P., Brown, J.C. & Steven, A.C. Three-dimensional structures of maturable and abortive capsids of equine herpesvirus 1 from cryoelectron microscopy. *J. Virol.* **64**, 563–573 (1990).
49. Booy, F.P. *et al.* Liquid-crystalline, phage-like packing of encapsidated DNA in Herpes Simplex Virus. *Cell* **64**, 1007–1015 (1991).
50. Booy, F.P., Trus, B.L., Davison, A.J. & Steven, A.C. The capsid architecture of Channel Catfish Virus, an evolutionarily distant herpesvirus, is largely conserved in the absence of discernible sequence homology with Herpes Simplex Virus. *Virology* **215**, 134–141 (1996).
51. Martino, R.L., Johnson, C.A., Suh, E.B., Trus, B.L. & Yap, T.K. Parallel computing in biomedical research. *Science* **265**, 902–908 (1994).
52. Johnson, C.A. *et al.* Orientation Determination in the 3D Reconstruction of Icosahedral Viruses using a Parallel Computer. in Suerpcomputing '94 B. Werner, Ed (IEEE Computer Society 550–559 , Washington, DC, 1994).
53. Marquardt, D.W. An Algorithm for Least Squares Estimation of Nonlinear Parameters. *J. Soc. Indust. Appl. Math.* **11**, 431–441 (1963).
54. Aldroubi, A., Trus, B.L., Unser, M., Booy, F.P. & Steven, A.C. Magnification mismatches between micrographs: corrective procedures and implications for structural analysis. *Ultramicroscopy* **46**, 175–188 (1992).
55. McKenna, R. *et al.* Atomic structure of single-stranded DNA bacteriophage ϕ174 and its functional implications. *Nature* **355**, 137–143 (1992).
56. Brünger, A.T. X-PLOR version 3.1. A system for X-ray crystallography and NMR, (Yale University Press, New Haven, CT, 1992).